

1 **The interaction of global motion and global form processing on the perception of implied**
2 **motion: an equivalent noise approach.**

3 **Mahesh R Joshi¹, Anita J Simmers², Seong T Jeon²**

4 **Affiliations:** ¹ Eye and Vision Research Group, School of Health Professions, University of Plymouth, Plymouth,
5 United Kingdom

6 ² Vision Sciences, Department of Life Sciences, Glasgow Caledonian University, Glasgow, United Kingdom

7
8 **Corresponding author:** Mahesh R Joshi; Mahesh.Joshi@plymouth.ac.uk

9
10 **Abstract**

11 Global motion and global form are proposed to be processed through functionally differentiated
12 independent channels along dorsal (motion) and ventral (form) pathways. However, more recent
13 studies show significant interactions between these pathways by inducing the perception of
14 motion (implied motion) from presenting the independent frames of static Glass patterns. The
15 mechanisms behind such interaction are not adequately understood with studies showing a larger
16 contribution of either a motion or form processing mechanism. In the current study, we adapted
17 the equivalent noise paradigm to disentangle the effect of internal noise (local processing) and
18 sampling efficiency (global processing) on global motion, global form, and the interaction of
19 both on the perception of implied motion using physically equivalent stimuli. Six visually normal
20 observers discriminated the direction or orientation of random dot kinematograms (RDK), static
21 Glass patterns (Glass), and dynamic Glass patterns (*d*Glass) whose directions/orientations were
22 determined by the means of normal distributions with a range of direction/orientation variances
23 that served as external noise. Thresholds (τ) showed a consistent pattern across observers and
24 external noise levels, where $\tau_{\text{Glass}} > \tau_{d\text{Glass}} > \tau_{\text{RDK}}$. Nested model comparisons where the thresholds
25 were related to the external noise, internal noise, and the sampling efficiency revealed that the
26 difference in performance between the tasks was best described by the change in sampling
27 efficiency with invariable internal noise ($ps < 0.01$). Our results showed that better sensitivity to
28 motion was not related to internal noise but better sampling efficiency at the global processing
29 stage. The results further suggested that higher thresholds for implied motion compared to real
30 motion could be due to inefficient pooling of local dipole orientation cues at global processing
31 stages involving motion mechanisms.

32 Introduction

33

34 Global motion and global form are proposed to be predominantly processed along independent
35 channels of dorsal and ventral streams (Braddick, Atkinson & Wattam-Bell, 2003, Braddick, et
36 al., 2001, Braddick, et al., 2002, Livingstone & Hubel, 1987, Milner & Goodale, 2008). Random
37 dot kinematograms (RDK) and Glass patterns (Glass, 1969) are commonly used stimuli to
38 evaluate global motion and form processing. Glass patterns are formed when an identical set of
39 random dot pattern is superimposed upon another, whereby one pattern is generated following a
40 linear or nonlinear transformation of the other pattern. (Glass, 1969) A variety of different spatial
41 patterns can be generated based on the angle of displacement by aligning the correlated pairs of
42 dots (dipoles) to a desired geometric transformation. The initial processing of motion/orientation
43 cues of individual dots/dipoles of RDK/Glass patterns occur in early cortical areas such as
44 V1/V2 – local processing (Dakin, 1997, Morrone, Burr & Vaina, 1995, Wilson & Wilkinson,
45 1998). This is followed by the global pooling of local motion/orientation resulting in the
46 perception of overall direction/orientation of the whole pattern in the higher cortical such as MT
47 for RDK (Morrone, Burr & Vaina, 1995) and V4 for Glass patterns (Dakin, 1997, Wilson &
48 Wilkinson, 1998) – global processing. More recently, however, it has been suggested that
49 interaction of information between motion and form is required for stable visual perception
50 where motion information can help perceive form better or vice versa (Donato, Pavan &
51 Campana, 2020, Goodale, 2011, Mather, et al., 2012, Ross, 2004, Ross, Badcock & Hayes, 2000,
52 Sincich & Horton, 2005). The most dramatic example of how motion influences form perception
53 is the demonstration of biological motion, where the biological form is only perceived when
54 motion cues are introduced to the static pattern of dots (Johansson, 1973). Biological motion is
55 believed to be processed along both motion and form processing channels but how much each
56 channel is responsible for the perception is still not clear (Giese & Poggio, 2003, Miller, Agnew
57 & Pilz, 2018). Another stimulus that relies on such interaction between motion and form cues is
58 the dynamic Glass pattern (Ross, Badcock & Hayes, 2000). Dynamic Glass patterns consist of
59 sequential display of independent, random sets of static Glass patterns with the same general
60 orientation (such as left translation) over time, this induces a compelling perception of motion
61 (implied motion) along the axis of global orientation of static Glass patterns (Ross, Badcock &
62 Hayes, 2000). The source of such perceived motion could only be from the underlying dipole

63 orientation of static Glass pattern structures as coherent motion vectors are absent in dynamic
64 Glass patterns.
65
66 The processing of implied motion is proposed to occur in areas V1 and V2 relying on a
67 mechanism similar to motion streaks (Burr & Ross, 2002, Ross, 2004). Motion streaks are static
68 image features that induce or accentuate the sense of motion, *e.g.* blurred static lines are
69 frequently used by artists to provide the impression of motion direction in still images. Geisler
70 (1999) proposed that moving objects leave a trail during temporal integration creating motion
71 streaks. The visual system utilises these motion streaks (form information) to disambiguate
72 object motion. The orientation selective cells in V1 are responsive to motion streaks.
73 Additionally, the outputs of both orientation and motion selective cells in V1 are combined to
74 form spatial motion direction (SMD) sensors that are sensitive to the orientation of the motion
75 streak and the motion direction (Geisler, 1999). The dipoles in the dynamic Glass patterns
76 "approximate small line segments" which form motion streaks and could stimulate the orientation
77 selective and SMD detectors in V1 (Burr & Ross, 2002, Ross, 2004). The involvement of V1 and
78 V2 neurones in decoding motion streaks in dynamic Glass patterns is further supported by the
79 finding of a proportion of motion sensitive cells in monkeys and humans that are responsive to
80 parallel motion (*i.e.* in the direction of their preferred orientation) instead of regularly
81 encountered cells which are responsive to an orthogonal motion (Apthorp, et al., 2013, Geisler,
82 et al., 2001). However, recent studies suggest that only local processing of dynamic Glass
83 patterns *i.e.* orientation of dipole pairs occurs at V1 (Donato, Pavan & Campana, 2020,
84 Krekelberg, Vatakis & Kourtzi, 2005, Ross, Badcock & Hayes, 2000) with global processing
85 occurring through the motion and form interaction within higher extra striate areas such as MT
86 (Kourtzi, Krekelberg & van Wezel, 2008, Li, et al., 2013, Mather et al., 2012, Pavan, Marotti &
87 Mather, 2013). Imaging studies (Krekelberg, et al., 2003, Krekelberg, Vatakis & Kourtzi, 2005)
88 reported that the motion selective cells in MT/MST respond similarly to the implied motion in
89 dynamic Glass patterns and the real motion in RDK. The inability of MT/MST cells to
90 differentiate between real and implied motion is why humans perceive motion in dynamic Glass
91 patterns (Krekelberg et al., 2003, Krekelberg, Vatakis & Kourtzi, 2005).

92

93 Behavioural studies have compared coherence threshold for implied motion (dynamic Glass
94 patterns) with thresholds for global form (static Glass patterns) and directional motion (RDK) to
95 understand the processing mechanism and interactions between these visual functions (Day &
96 Palomares, 2014, Nankoo, et al., 2012, Nankoo, et al., 2015). The coherence thresholds for
97 dynamic Glass patterns are lower compared to static Glass patterns but higher than the real
98 motion in RDK (Nankoo et al., 2012). The coherence thresholds for dynamic Glass patterns
99 varied according to the pattern type (higher thresholds for translation compared to radial and
100 rotational) similar to the static Glass patterns. This finding was reported as evidence of a larger
101 influence of the form processing mechanism on implied motion processing (Nankoo et al., 2012).
102 However, another study showed that the coherence thresholds reduced linearly with the increase
103 in the temporal frequency of dynamic Glass patterns, suggesting that the processing mechanism
104 relies more on the temporal properties (Day & Palomares, 2014). Hence the processing of
105 implied motion and how it is influenced by motion and form processing mechanisms are still not
106 clear. The coherence threshold is measured as the minimum fraction of signal elements required
107 for the detection of coherent motion/orientation in the presence of random noise (Newsome &
108 Pare, 1988). Another behavioural method that can be used to evaluate the processing of dynamic
109 Glass patterns in relation to motion (RDK) and form (Glass patterns) processing is the equivalent
110 noise paradigm (Watamaniuk & Sekuler, 1992). In the equivalent noise paradigm, the
111 direction/orientation of individual elements is derived from a Gaussian distribution with a
112 prescribed mean and standard deviation (Watamaniuk & Sekuler, 1992) where all individual
113 elements are assigned with independent local directions/orientations along the mean of the
114 underlying distribution. In such an arrangement, the dot/dipole elements act as signal (average
115 direction/orientation of the elements) and noise (average dispersion of the individual element's
116 direction/orientation from the mean) at the same time. Thresholds measured at variable noise can
117 then be fit to a linear amplifier model of the equivalent noise paradigm to separate the observer's
118 performance into internal noise and sampling efficiency parameters (Pelli, 1981, Pelli & Farell,
119 1999). For the RDK and Glass patterns, the internal noise derived from the equivalent noise
120 paradigm represents the local variance in direction of motion (RDK) and orientation (Glass
121 patterns) of individual elements – local processing (Dakin, Mareschal & Bex, 2005). The
122 sampling efficiency meanwhile represents the number of elements the visual system summates to
123 provide an overall global percept – global processing (Dakin, Mareschal & Bex, 2005). The

124 equivalent noise paradigm can hence provide better insight into the interaction of motion and
125 form processing at both local and global processing levels.

126
127 In this study, we adapted the equivalent noise paradigm to investigate sensitivity to implied
128 motion and compared that to motion and form thresholds using physically equivalent stimuli in
129 order to better understand the contribution of global motion and form on the perception of
130 implied motion at local and global processing stages.

131

132 **Methods**

133 **Participants**

134 A total of 6 participants (mean age \pm SD = 31.66 \pm 6.86 years) with normal or corrected to
135 normal visual acuity (6/6) participated in the study. Four of the six participants were naïve to the
136 purpose of the experiment while two were psychophysically experienced observers. Written
137 informed consent was obtained from each participant and the experiments were carried out in
138 accordance with The Code of Ethics of the World Medical Association, Declaration of Helsinki.
139 The study protocol was approved by the Life Sciences Human Subjects Research Ethics
140 Committee of Glasgow Caledonian University.

141

142 **Stimuli**

143 The global motion, global form, and implied motion were investigated using random dot
144 kinematograms, Glass patterns and dynamic Glass patterns respectively. The stimuli were
145 generated using MATLAB (MATLAB, 2009) with Psychophysics Toolbox extensions
146 (Brainard, 1997, [Kleiner, et al., 2007](#), Pelli, 1997) and displayed on a 21" CRT monitor
147 (resolution of 1920 x 1440 pixels and refresh rate of 75Hz). The three stimuli shared the same
148 physical characteristics. They were composed of 500 black dots (0.083° in diameter) presented in
149 a circular aperture (10° in diameter at 50 cm) at the centre of the monitor with a dot density of
150 12.81 dots/deg². The mean background luminance of the display was 35cd/m² and the contrast of
151 the dot elements was 95% Michelson contrast.

152

153

154

155 **RDK**

156 The RDKs were presented for 38 frames over the display time of 0.5 sec. All dots followed a
157 defined trajectory for 6 frames (0.08 sec) at a dot speed of $10^\circ/\text{sec}$ after which they disappeared
158 and were generated at a random location within the stimulus area.

159

160 **Glass pattern**

161 The Glass patterns were generated by randomly placing 250 black dots at the centre of the
162 display. Another identical set of 250 dots was then superimposed after a linear geometrical
163 transformation. The corresponding dot elements of the pattern were separated by a distance of
164 0.133° , which was scaled to the distance travelled by the dots in the RDK in two consecutive
165 frames (dot speed of $10^\circ/\text{s}$ for 0.5 sec with a monitor refresh rate of 75 frames/s).

166

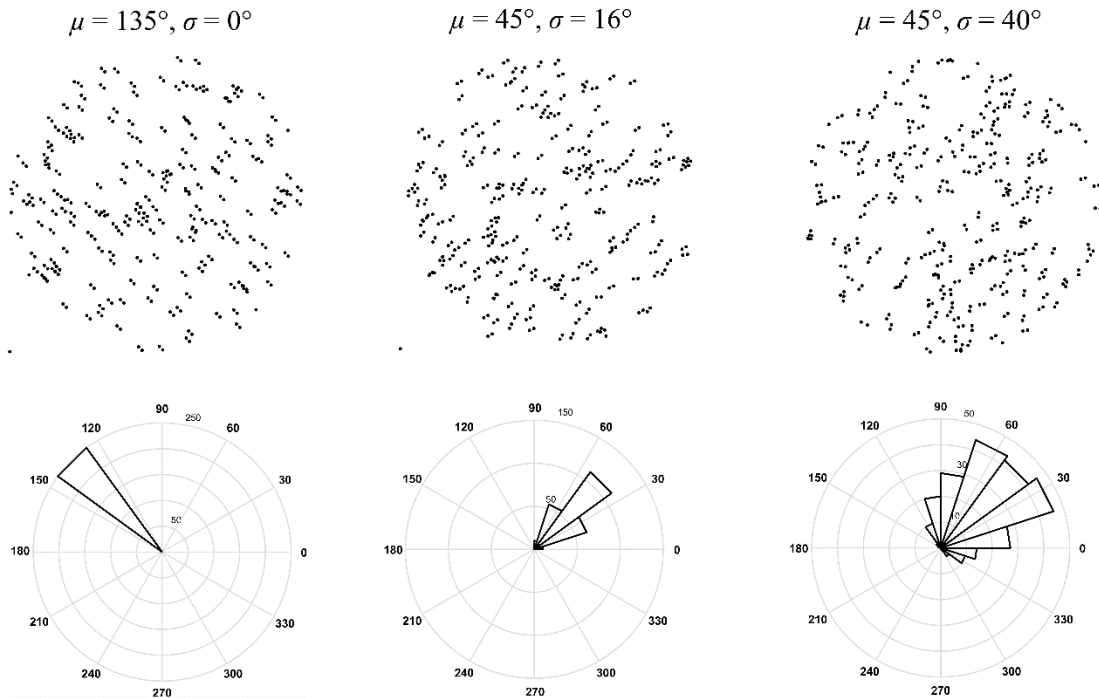
167 **Dynamic Glass pattern**

168 Dynamic Glass patterns were composed of 9 independently generated static Glass patterns with
169 similar physical parameters to that previously described for the static Glass patterns. Each static
170 Glass pattern remained on the screen for 6 frames before being replaced by another
171 independently generated static Glass pattern. The total stimulus duration was 0.5s.

172

173 The direction of motion/orientation of individual dots/dipoles in RDK, Glass patterns, and
174 dynamic Glass patterns was generated from a standard Gaussian distribution with a prescribed
175 mean and standard deviation. The mean and standard deviation of the distribution was changed
176 to vary the angle from the vertical reference (90°) and added external noise respectively across
177 the trials. The overall direction of motion of the RDK/orientation in Glass patterns (right or left
178 from vertical) was randomised (Figure 1). Eight external noise levels were used for the
179 experiments: 0° , 2° , 4° , 8° , 16° , 24° , 32° , and 40° .

180



181
 182 Figure 1: Examples of Glass patterns with differing orientation and noise levels (top panels). The orientations of
 183 individual dipoles in each Glass pattern were generated from a Gaussian distribution (shown in angle histograms,
 184 bottom panels). The mean (μ) of the distribution ($\pm 45^\circ$ from the vertical here) represents the global orientation of the
 185 Glass patterns. The added external noise was varied by changing the standard deviation (σ) of the distribution (from
 186 left to right panels, 0° , 16° , and 40°). The task for the observer was to discriminate the overall orientation of Glass
 187 patterns. For the RDK, individual dots followed the directional trajectory generated from the Gaussian distribution.
 188 For dynamic Glass patterns, nine frames of independent static Glass patterns were displayed over the stimulus
 189 duration.

190
 191 **Procedure**

192 Participants completed five sessions of the psychophysical experiment for three stimuli
 193 binocularly. Each experiment started with the presentation of a white fixation dot (0.2° diameter)
 194 at the centre of the screen, followed by the presentation of either Glass patterns, dynamic Glass
 195 patterns or RDK for 0.5 sec. The participant's task in each trial was to discriminate the overall
 196 orientation/IMPLIED motion/direction of the Glass pattern/dynamic Glass pattern/RDK from the
 197 vertical reference (90°). Only the negative response feedback was provided.

198 Eight 3:1 interleaved staircases (Wetherill and Levitt, 1965) were used for stimulus presentation
 199 and data collection. The staircase for each external noise level started with an overall mean
 200 orientation or direction of 30° from the vertical. The initial step size for stimulus intensity
 201 adjustment was an octave which was reduced to half an octave and further to a quarter of an

202 octave after three and six reversals respectively. Each staircase terminated after the completion
 203 of ten reversals or 100 trials, whichever occurred first and the threshold was calculated as the
 204 geometrical mean of the last seven reversals. All participants completed two sessions of 15
 205 practice trials for each external noise conditions followed by five full experimental sessions for
 206 three stimuli.

207

208 The thresholds (τ_o) at eight external noise levels (σ_{ext}) were modelled by the equation below to
 209 relate the performance into internal equivalent noise (σ_{eq}) and sampling efficiency (Eff)
 210 parameters (Pelli, 1981, Pelli & Farell, 1999).

$$211 \quad \tau_o = \sqrt{\frac{\sigma_{eq}^2 + \sigma_{ext}^2}{Eff}} \quad (1)$$

212

213 The threshold data were then used to fit various nested models. The full model contained six
 214 parameters (2 each of σ_{eq} and Eff for Glass patterns, dynamic Glass patterns, and RDK). The
 215 fitting models were then reduced by constraining the parameters (either σ_{eq} and Eff or both across
 216 the three stimuli), resulting in different nested models. The best model to describe the threshold
 217 data was selected by testing the goodness of fits between the nested models hierarchically with
 218 the following equation.

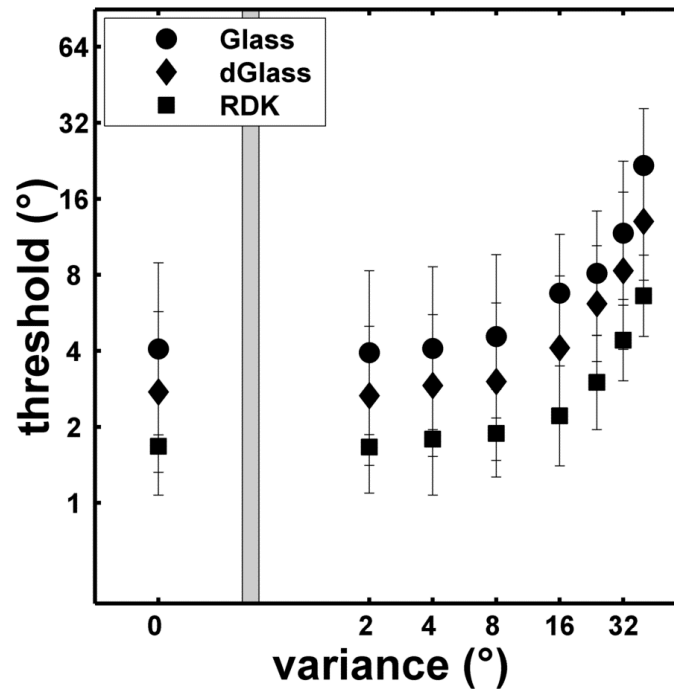
$$219 \quad F(df_1, df_2) = \frac{r_{full}^2 - r_{reduced}^2 / df_1}{1 - r_{full}^2 / df_2} \quad (2)$$

220 Where, $df_1 = k_{full} - k_{reduced}$ and $df_2 = N - k_{full}$. k is the number of parameters in each model,
 221 and N is the number of predicted data points.

222

223 **Results:**

224 The mean implied motion thresholds for dynamic Glass patterns ($dGlass$) were higher than the
 225 mean thresholds for the RDK but lower than those for the Glass patterns at all external noise
 226 levels (Figure 2). For all stimuli, when thresholds were plotted against the external noise in the
 227 logarithmic scale, thresholds were low and similar at lower noise levels and started to increase at
 228 noise levels of 8° and 16° with the highest thresholds for the 40° variance.



230

231 Figure 2: Mean orientation/implicit motion/directional motion discrimination thresholds ($n = 6$) at eight noise levels
 232 for Glass patterns, dynamic Glass patterns and RDK. The error bar represents ± 1 standard deviation and the grey bar
 233 represents axis break.

234

235 The individual and mean thresholds were used to fit the linear amplifier model. Various nested
 236 models were tested from the full model (with 3 sets of independent σ_{eq} and Eff) to the most
 237 parsimonious model (with a single set of σ_{eq} and Eff) across the three stimuli (see Table 1 and
 238 Figure 3).

239

Participants	S1	S2	S3	S4	S5	S6	Average
Full model							
σ_{eq} Glass	11.05°	24.91°	9.24°	5.22°	9.51°	8.95°	10.06°
σ_{eq} dGlass	10.45°	12.24°	10.01°	8.44°	12.38°	9.01°	10.32°
σ_{eq} RDK	10.39°	16.61°	13.22°	8.65°	19.45°	12.50°	12.86°
Eff Glass	1.51	2.56	2.40	3.75	3.46	3.38	2.64
Eff dGlass	3.19	3.30	1.80	7.83	4.90	5.48	3.97
Eff RDK	5.77	8.64	6.87	7.92	8.63	11.40	7.91
r^2	0.94	0.94	0.95	0.94	0.83	0.97	0.97
Reduced model-1 with σ_{eq} constrained							
σ_{eq}	10.63°	16.91°	10.75°	7.27°	12.70°	10.06°	11.00°

<i>Eff</i> Glass	1.48	1.97	2.58	4.29	4.03	3.58	2.76
<i>Eff</i> dGlass	3.22	3.99	1.86	7.32	4.97	5.78	4.10
<i>Eff</i> RDK	5.83	8.74	6.15	7.31	6.67	10.10	7.27
r^2	0.94	0.90	0.94	0.92	0.80	0.96	0.96
$F(2,18)$	0.03*	2.12*	1.06*	2.30*	1.92*	2.19*	1.10*
Reduced model-2 with <i>Eff</i> constrained							
σ_{eq} Glass	38.95°	67.54°	17.98°	10.51°	15.68°	24.73°	23.10°
σ_{eq} dGlass	13.33°	26.51°	26.22°	6.42°	13.38°	12.30°	13.55°
σ_{eq} RDK	6.32°	10.83°	6.92°	6.60°	10.69°	7.06°	7.33°
<i>Eff</i>	3.89	5.99	3.94	6.29	5.21	6.99	4.92
r^2	0.81	0.83	0.75	0.84	0.71	0.80	0.81
$F(2,18)$	19.32	11.13	33.32	14.89	6.85	48.84	42.92
Simplest reduced model with both σ_{eq} and <i>Eff</i> constrained							
σ_{eq}	10.63°	16.91°	10.75°	7.27°	12.70°	10.06°	11.00°
<i>Eff</i>	3.03	4.10	3.09	6.12	5.11	5.94	4.35
r^2	0.45	0.25	0.49	0.81	0.67	0.59	0.61
$F(2,18)†$	37.34	39.20	38.74	9.73	4.31	55.22	49.07
$F(2,20)‡$	82.96	84.75	84.91	19.06	7.44	120.28	107.83

240

241 **Table 1: The best fitting parameters and r^2 values for model fits to individual and mean threshold data for**
 242 **Glass, dGlass, and RDK.**

243

244 *The values in the top section are the results of the fits with six free parameters (one σ_{eq} and *Eff* each for Glass,*
 245 *dGlass, and RDK). The second and third sections show the results with σ_{eq} and *Eff* fixed respectively across Glass,*
 246 *dGlass, and RDK. The bottom section shows results with both σ_{eq} and *Eff* fixed across the conditions. The *F* scores*
 247 *are the result of a nested hypothesis test between restricted models (4-parameter or 2-parameter models) and the*
 248 *full models (6-parameter or 4-parameter models).*

249

250 * = *F* scores which resulted in no significant difference ($p > 0.05$) in the goodness of the fit measure with the
 251 reduced model (here 1 σ_{eq} , 3 *Eff*) compared to the full model (3 σ_{eq} , 3 *Eff*). The rest of the *F* scores represent a
 252 poorer fit ($p < 0.05$) compared to the full model (1 σ_{eq} , 3 *Eff*).

253 † = *F* statistics of the simplest model (1 σ_{eq} , 1 *Eff*) compared to full model (3 σ_{eq} , 3 *Eff*)

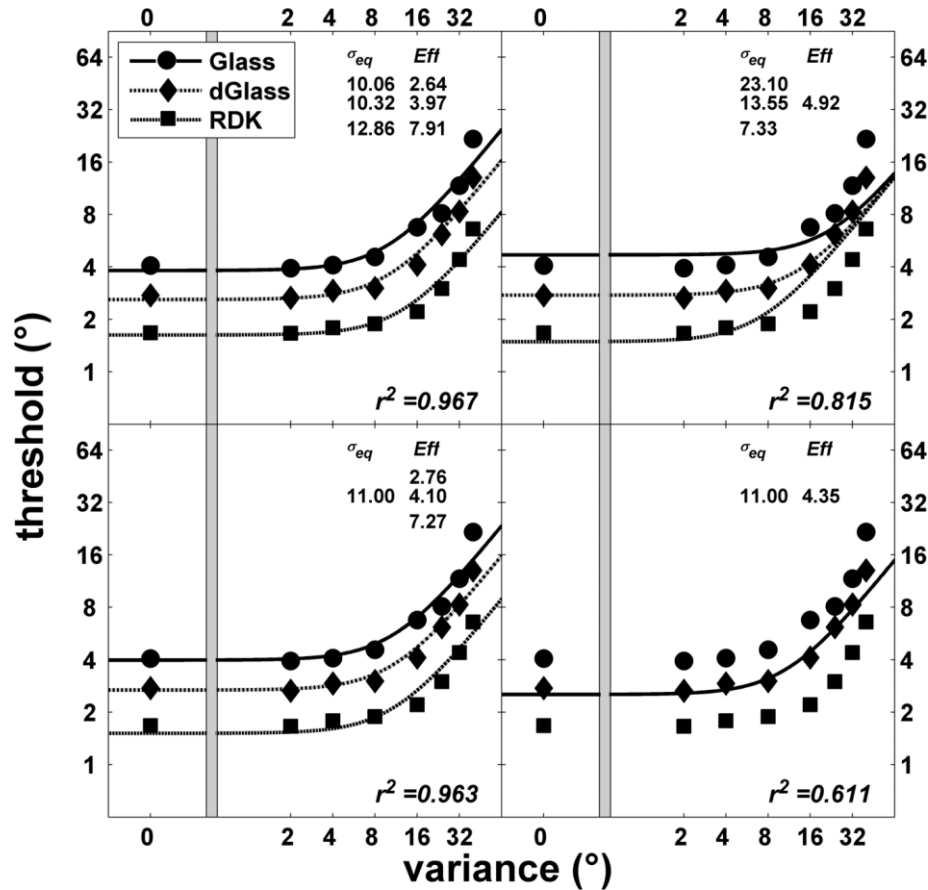
254 ‡ = *F* statistics of the simplest model (1 σ_{eq} , 1 *Eff*) compared to the model selected from the first stage of comparison
 255 (1 σ_{eq} , 3 *Eff*)

256

257 Among the reduced models for mean thresholds, the goodness of fit (r^2) with one σ_{eq} and three
 258 *Eff* was equivalent to the full model (three σ_{eq} and three *Eff*) ($F(2,18) = 1.10$, $p > 0.1$). The fits
 259 with three σ_{eq} and one *Eff* ($F(2,18) = 42.92$, $p < 0.01$) and one σ_{eq} and one *Eff* ($F(2,18) = 49.07$, p
 260 < 0.01) meanwhile resulted in poorer fits compared to the full model. A further test with one σ_{eq}
 261 and three *Eff* as the full model and one σ_{eq} and one *Eff* as the reduced model showed that the

262 reduced model resulted in a significantly poorer fit ($F(2,20) = 107.83, p < 0.01$). The same
 263 pattern of result was obtained for all individual observers. (Table 1) The result confirmed that the
 264 model with one σ_{eq} and three Eff best described the performance of the observers across the three
 265 stimulus types.

266



267

268 **Figure 3: Nested models relating the mean thresholds to different values of internal noise and sampling**
 269 **efficiency for Glass, dGlass, and RDK.**

270 *Top left: the full model with independent σ_{eq} and Eff for three stimuli. Top right: the constrained model with*
 271 *independent σ_{eq} and a single Eff parameter. Bottom left: the constrained model with independent Eff and a single σ_{eq}*
 272 *parameter. Bottom right: the simplest reduced model with both σ_{eq} and Eff constrained. The reduced model with one*
 273 *σ_{eq} and three Eff (bottom left) resulted in no significant difference ($p > 0.05$) in the goodness of the fit measure (r^2)*
 274 *compared to the full model.*

275

276 Discussion:

277 Global motion vs. Global form

278 The mean fine discrimination thresholds (*i.e.*, discrimination threshold from the vertical at no
 279 noise condition) for the direction of motion in the RDK and the orientation of the dipole Glass

280 patterns were $1.85^\circ (\pm 0.89^\circ)$ and $5.62^\circ (\pm 5.76^\circ)$ respectively. Our results are in agreement with
281 previous studies that showed similar fine motion direction discrimination thresholds for young
282 adults (Bocheva, Angelova & Stefanova, 2013, Bogfjellmo, Bex & Falkenberg, 2014). As far as
283 we are aware there are no reports on fine orientation discrimination thresholds using Glass
284 patterns. The orientation discrimination thresholds (Glass patterns) were consistently higher than
285 that for the direction of motion (RDK) at all levels of added external noise which is in line with
286 previous studies measuring coherence threshold using physically comparable Glass patterns
287 (Ditchfield, McKendrick & Badcock, 2006, Nankoo et al., 2012) and line streaks (Simmers,
288 Ledgeway & Hess, 2005, Simmers, et al., 2003, Simmers, et al., 2006). We further probed the
289 better performance for motion processing with the equivalent noise paradigm to parse out the
290 effects of local and global processing mechanisms. Internal equivalent noise and sampling
291 efficiency for the mean direction discrimination thresholds were 12.86° and 8 elements
292 respectively. Previous studies have reported the internal noise in the motion domain ranging
293 from 2.97° to 25° (Bocheva, Angelova & Stefanova, 2013, Dakin, Mareschal & Bex, 2005,
294 Watamaniuk & Sekuler, 1992). The difference might be reflective of the stimulus differences in
295 these studies as has been reported before (Bocheva, Angelova & Stefanova, 2013, Dakin,
296 Mareschal & Bex, 2005). There are no previous reports on the internal noise and sampling
297 efficiency employing Glass patterns. A study using Gabor patches reported equivalent internal
298 noise in the range of 4.4° - 7.8° (Dakin, 2001).

299
300 Our result of similar internal equivalent noise in motion and form domains suggests that both
301 pathways might share similar local processing limitations with differences in the performance
302 due to the improved efficiency in the global motion processing mechanism. Various studies
303 suggest that the local processing of dot motion in RDK (Morrone, Burr & Vaina, 1995, Nishida,
304 2011) and dipole orientation in Glass patterns (Smith, Bair & Movshon, 2002, Smith, Kohn &
305 Movshon, 2007, Wilson & Wilkinson, 1998, Wilson, Wilkinson & Asaad, 1997, Wilson, Switkes
306 & De Valois, 2004) occur in area V1/V2 with global processing occurring in areas of MT and
307 V4. The common physiological limitations in the local processing area could have resulted in the
308 similar internal equivalent noise observed in both domains. The sampling efficiency parameter
309 refers to the visual system's ability to pool local directional/orientation information from the
310 individual dot and dipole elements (Dakin, Mareschal & Bex, 2005). Another method used to

311 study the pooling of motion/orientation signals is by restricting the coherent elements in the
312 RDK and Glass patterns to wedge shaped areas of varying size within the stimulus. The
313 discrimination threshold for a translation RDK improved linearly with the increase in the size of
314 the signal area, implying global spatial summation of almost 100% (Morrone, Burr & Vaina,
315 1995) while for the translation Glass patterns, the global summation ranged between 25-33%
316 (Wilson & Wilkinson, 1998). The better sampling efficiency along the motion pathway in the
317 current study albeit using a different experimental paradigm is in line with the previous findings
318 of a larger global pooling for motion processing than form processing (Morrone, Burr & Vaina,
319 1995, Wilson & Wilkinson, 1998).

320

321 **Implied motion vs. Global motion vs. Global form**

322

323 The implied motion thresholds for the dynamic Glass patterns were lower than those for the
324 static Glass patterns but higher than the RDK at all external noise levels. As far as we know, no
325 study has evaluated the sensitivity to dynamic Glass patterns using the equivalent noise
326 paradigm. Other studies have reported lower coherence thresholds for dynamic Glass patterns
327 compared to the static Glass patterns (Burr & Ross, 2006, Nankoo et al., 2012, Nankoo et al.,
328 2015). The reduced thresholds for the dynamic Glass patterns could be due to the activation of
329 the motion streak mechanism (Ross, 2004, Ross, Badcock & Hayes, 2000) that may be present at
330 the early cortical visual areas of V1 and V2 (Apthorp et al., 2013, Burr & Ross, 2002) and the
331 later global processing areas of MT and MST (Krekelberg, Vatakis & Kourtzi, 2005, Mather et
332 al., 2012, Pavan, Marotti & Mather, 2013). Another possible reason for better sensitivity to
333 implied motion in dynamic Glass patterns compared to the static Glass patterns could be due to
334 the summation of information from multiple independent static Glass patterns over time (Nankoo
335 et al., 2015). Two factors are involved in such improvement: the accumulation of form
336 information from multiple static Glass patterns (Nankoo et al., 2012, Nankoo et al., 2015) and
337 the influence of temporal frequency of the presentation (Day & Palomares, 2014). The coherence
338 thresholds for the dynamic Glass patterns varied according to the pattern types (translation,
339 radial, and rotation) as observed for the static Glass patterns while the motion coherence
340 thresholds were similar for all three RDK types (Nankoo et al., 2012). The result hence
341 emphasised a larger role for the form processing mechanism (Nankoo et al., 2012). However,

342 other studies have reported that the motion coherence thresholds for RDK also vary depending
343 upon the pattern types, especially at slower speeds (Freeman & Harris, 1992, Lee & Lu, 2010).
344 In another study, coherence thresholds for dynamic Glass patterns reduced linearly with the
345 increase in temporal frequency suggesting the importance of temporal properties (Day &
346 Palomares, 2014). However, on independently varying the temporal frequency and the number of
347 unique frames, the number of frames was still more influential in threshold reduction (Nankoo et
348 al., 2015).

349
350 The similar level of internal noise observed for different stimuli (RDK, dynamic Glass and Glass
351 patterns) suggests that local processing (in both the motion and form domain) may share a
352 common local level processing of dot motion and dipole orientation. The finding that the
353 perception of both static and dynamic Glass patterns are lost when the dipoles are of opposite
354 polarity (Or, Khuu & Hayes, 2007) further suggests that both patterns share similar local level
355 processing. Motion streak detectors present in the primary visual cortex are proposed to be
356 responsible for the processing of implied motion in line streaks (Geisler, 1999). The similar
357 internal noise observed here between dynamic Glass patterns and static Glass patterns in which
358 motion streak is absent and between dynamic Glass and RDK in which motion streak detectors
359 would be more influential suggests that motion streak mechanism in V1 might not be adequate to
360 explain the implied motion perceived in dynamic Glass patterns.

361
362 The difference in the performance for three stimulus types was best represented by the change in
363 the global processing parameter, the sampling efficiency. The motion sensitive cells in MT/MST
364 respond similarly to both real motion and implied motion (Krekelberg et al., 2003, Krekelberg,
365 Vatakis & Kourtzi, 2005) and may well be involved in the global processing of the implied
366 motion in dynamic Glass patterns. The motion-form interactions similar to that proposed for the
367 motion streak mechanism are also present at the global processing levels of MT (Mather et al.,
368 2012) and MST (Pavan, Marotti & Mather, 2013), and such interactions could have influenced
369 the differences in the sampling efficiency observed here. Furthermore, some MT cells responsive
370 to orthogonal motion, change their preference over time to that of parallel motion (in the
371 direction of the motion streak) starting from around 75ms of the stimulus onset (Pack & Born,
372 2001). This change in sensitivity could be influential in processing the motion streaks left behind

373 by the fast moving objects (Burr & Ross, 2002). Our results show that any facilitation of implied
374 motion processing due to the interaction of motion and form processing streams in line with the
375 motion streak mechanism may well extend to the global processing level. However, the
376 mechanism may not be as efficient as that for directional motion in RDK. From our results of
377 constant internal noise and a difference in sampling efficiency and previous literature, we
378 speculate that the local processing of dipole orientation in dynamic Glass patterns is similar to
379 the processing of static Glass patterns (extracting dipole orientation) with further global
380 processing most likely occurring along the motion processing areas of MT/MST. Such an
381 assumption is supported by a series of imaging and motion adaptation studies. Imaging studies
382 report that the motion responsive neurones along the ventral stream are not responsive to the
383 implied motion in dynamic Glass patterns (Krekelberg et al., 2003, Krekelberg, Vatakis &
384 Kourtzi, 2005) suggesting that any contribution from the form processing pathway to the
385 processing of dynamic Glass patterns is mostly limited to the local extraction of dipole
386 orientation. The notion of the involvement of MT in global processing of dynamic Glass patterns
387 is also supported by adaptation studies. The perceived direction of motion streaks is affected by
388 adaptation to a wide range of static orientations (Tang, et al., 2015). This range was broader than
389 what could be accounted for by the neuronal properties of V1. Furthermore, this range closely
390 approximated the broad bandwidths of motion selective cells in area MT. Based on these
391 findings an alternate model was proposed, where the orientation cues are initially processed at
392 the V1 level with the second stage of motion processing occurring at area MT (Tang et al.,
393 2015). The model predictions are in line with our findings of similar internal equivalent noise
394 and differences in sampling efficiency for dynamic Glass patterns compared to both RDK and
395 static Glass patterns.

396

397 Our results show that humans have better sensitivity to global implied motion compared to
398 global form but lower than that for global motion. The results further suggest that higher
399 thresholds for implied motion compared to real motion is due to differences in sampling
400 efficiency which could be due to inefficient pooling of local cues of implied motion at the global
401 processing stage.

402

403

404 **References:**

- 405
- 406 Apthorp, D., Schwarzkopf, D.S., Kaul, C., Bahrami, B., Alais, D., & Rees, G. (2013). Direct evidence for
407 encoding of motion streaks in human visual cortex. *Proceedings of the Royal Society B: Biological*
408 *Sciences*, 280 (1752), 20122339.
- 409 Bocheva, N., Angelova, D., & Stefanova, M. (2013). Age-related changes in fine motion direction
410 discriminations. *Experimental Brain Research*, 228 (3), 257-278.
- 411 Bogfjellmo, L.G., Bex, P.J., & Falkenberg, H.K. (2014). The development of global motion discrimination
412 in school aged children. *Journal of Vision*, 14 (2)
- 413 Braddick, O., Atkinson, J., & Wattam-Bell, J. (2003). Normal and anomalous development of visual
414 motion processing: motion coherence and 'dorsal-stream vulnerability'. *Neuropsychologia*, 41 (13),
415 1769-1784.
- 416 Braddick, O.J., O'Brien, J.M., Wattam-Bell, J., Atkinson, J., Hartley, T., & Turner, R. (2001). Brain areas
417 sensitive to coherent visual motion. *Perception*, 30 (1), 61-72.
- 418 Braddick, O.J., O'Brien, J.M.D., Rees, G., Wattam-Bell, J., Atkinson, J., & Turner, R. (2002). Quantitative
419 neural responses to form coherence in human extrastriate cortex. *Society for Neuroscience 32nd Annual*
420 *Meeting* (Washington, DC).
- 421 Brainard, D.H. (1997). The Psychophysics Toolbox. *Spatial Vision*, 10 (4), 433-436.
- 422 Burr, D., & Ross, J. (2006). The effects of opposite-polarity dipoles on the detection of Glass patterns.
423 *Vision Res*, 46 (6-7), 1139-1144.
- 424 Burr, D.C., & Ross, J. (2002). Direct Evidence That "Speedlines" Influence Motion Mechanisms. *The*
425 *Journal of Neuroscience*, 22 (19), 8661-8664.
- 426 Dakin, S.C. (1997). The detection of structure in glass patterns: Psychophysics and computational
427 models. *Vision Research*, 37 (16), 2227-2246.
- 428 Dakin, S.C. (2001). Information limit on the spatial integration of local orientation signals. *Journal of the*
429 *Optical Society of America. A, Optics, image science, and vision*, 18 (5), 1016-1026.
- 430 Dakin, S.C., Mareschal, I., & Bex, P.J. (2005). Local and global limitations on direction integration
431 assessed using equivalent noise analysis. *Vision Research*, 45 (24), 3027-3049.
- 432 Day, A.M., & Palomares, M. (2014). How temporal frequency affects global form coherence in Glass
433 patterns. *Vision Research*, 95 (0), 18-22.
- 434 Ditchfield, J.A., McKendrick, A.M., & Badcock, D.R. (2006). Processing of global form and motion in
435 migraineurs. *Vision Research*, 46 (1-2), 141-148.
- 436 Donato, R., Pavan, A., & Campana, G. (2020). Investigating the Interaction Between Form and Motion
437 Processing: A Review of Basic Research and Clinical Evidence. *Frontiers in Psychology*, 11 (2867)
- 438 Freeman, T.C., & Harris, M.G. (1992). Human sensitivity to expanding and rotating motion: effects of
439 complementary masking and directional structure. *Vision Research*, 32 (1), 81-87.
- 440 Geisler, W.S. (1999). Motion streaks provide a spatial code for motion direction. *Nature*, 400 (6739), 65-
441 69.
- 442 Geisler, W.S., Albrecht, D.G., Crane, A.M., & Stern, L. (2001). Motion direction signals in the primary
443 visual cortex of cat and monkey. *Visual Neuroscience*, 18 (04), 501-516.
- 444 Giese, M.A., & Poggio, T. (2003). Neural mechanisms for the recognition of biological movements.
445 *Nature Reviews Neuroscience*, 4 (3), 179-192.
- 446 Glass, L. (1969). Moire effect from random dots. *Nature*, 223 (5206), 578-580.
- 447 Goodale, M.A. (2011). Transforming vision into action. *Vision Research*, 51 (13), 1567-1587.
- 448 Johansson, G. (1973). Visual perception of biological motion and a model for its analysis. *Perception &*
449 *Psychophysics*, 14 (2), 201-211.

450 Kleiner, M., Brainard, D., Pelli, D., Ingling, A., Murray, R., & Broussard, C. (2007). What's new in
451 Psychtoolbox-3? *Perception*, *36*, 1-16.

452 Kourtzi, Z., Krekelberg, B., & van Wezel, R.J. (2008). Linking form and motion in the primate brain. *Trends*
453 *in Cognitive Sciences*, *12* (6), 230-236.

454 Krekelberg, B., Dannenberg, S., Hoffmann, K.-P., Bremmer, F., & Ross, J. (2003). Neural correlates of
455 implied motion. *Nature*, *424* (6949), 674-677.

456 Krekelberg, B., Vatakis, A., & Kourtzi, Z. (2005). Implied motion from form in the human visual cortex.
457 *Journal of Neurophysiology*, *94* (6), 4373-4386.

458 Lee, A.L., & Lu, H. (2010). A comparison of global motion perception using a multiple-aperture stimulus.
459 *Journal of Vision*, *10* (4), 9 1-16.

460 Li, P., Zhu, S., Chen, M., Han, C., Xu, H., Hu, J., Fang, Y., & Lu, Haidong D. (2013). A Motion Direction
461 Preference Map in Monkey V4. *Neuron*, *78* (2), 376-388.

462 Livingstone, M., & Hubel, D. (1987). Psychophysical evidence for separate channels for the perception of
463 form, color, movement, and depth. *The Journal of Neuroscience*, *7* (11), 3416-3468.

464 Mather, G., Pavan, A., Bellacosa, R.M., & Casco, C. (2012). Psychophysical evidence for interactions
465 between visual motion and form processing at the level of motion integrating receptive fields.
466 *Neuropsychologia*, *50* (1), 153-159.

467 MATLAB (2009). version 7.9.0.529 (R2009b). (Natick, Massachusetts: The MathWorks Inc.

468 Miller, L., Agnew, H.C., & Pilz, K.S. (2018). Behavioural evidence for distinct mechanisms related to global
469 and biological motion perception. *Vision Research*, *142*, 58-64.

470 Milner, A.D., & Goodale, M.A. (2008). Two visual systems re-viewed. *Neuropsychologia*, *46* (3), 774-785.

471 Morrone, M.C., Burr, D.C., & Vaina, L.M. (1995). Two stages of visual processing for radial and circular
472 motion. *Nature*, *376* (6540), 507-509.

473 Nankoo, J.-F., Madan, C.R., Spetch, M.L., & Wylie, D.R. (2012). Perception of dynamic Glass patterns.
474 *Vision Research*, *72* (0), 55-62.

475 Nankoo, J.-F., Madan, C.R., Spetch, M.L., & Wylie, D.R. (2015). Temporal summation of global form
476 signals in dynamic Glass patterns. *Vision Research*, *107* (0), 30-35.

477 Newsome, W., & Pare, E. (1988). A selective impairment of motion perception following lesions of the
478 middle temporal visual area (MT). *The Journal of Neuroscience*, *8* (6), 2201-2211.

479 Nishida, S.y. (2011). Advancement of motion psychophysics: Review 2001–2010. *Journal of Vision*, *11*
480 (5), 11-11.

481 Or, C.C., Khuu, S.K., & Hayes, A. (2007). The role of luminance contrast in the detection of global
482 structure in static and dynamic, same- and opposite-polarity, Glass patterns. *Vision Research*, *47* (2),
483 253-259.

484 Pack, C.C., & Born, R.T. (2001). Temporal dynamics of a neural solution to the aperture problem in visual
485 area MT of macaque brain. *Nature*, *409* (6823), 1040-1042.

486 Pavan, A., Marotti, R.B., & Mather, G. (2013). Motion-form interactions beyond the motion integration
487 level: Evidence for interactions between orientation and optic flow signals. *Journal of Vision*, *13* (6), 16-
488 16.

489 Pelli, D.G. (1981). Effects of Visual Noise. PhD (Cambridge: Cambridge University.

490 Pelli, D.G. (1997). The VideoToolbox software for visual psychophysics: transforming numbers into
491 movies. *Spatial Vision*, *10* (4), 437-442.

492 Pelli, D.G., & Farell, B. (1999). Why use noise? *Journal of the Optical Society of America. A, Optics, image*
493 *science, and vision*, *16* (3), 647-653.

494 Ross, J. (2004). The perceived direction and speed of global motion in Glass pattern sequences. *Vision*
495 *Research*, *44* (5), 441-448.

496 Ross, J., Badcock, D.R., & Hayes, A. (2000). Coherent global motion in the absence of coherent velocity
497 signals. *Current Biology*, *10* (11), 679-682.

498 Simmers, A.J., Ledgeway, T., & Hess, R.F. (2005). The influences of visibility and anomalous integration
499 processes on the perception of global spatial form versus motion in human amblyopia. *Vision Research*,
500 45 (4), 449-460.

501 Simmers, A.J., Ledgeway, T., Hess, R.F., & McGraw, P.V. (2003). Deficits to global motion processing in
502 human amblyopia. *Vision Research*, 43 (6), 729-738.

503 Simmers, A.J., Ledgeway, T., Mansouri, B., Hutchinson, C.V., & Hess, R.F. (2006). The extent of the dorsal
504 extra-striate deficit in amblyopia. *Vision Research*, 46 (16), 2571-2580.

505 Sincich, L.C., & Horton, J.C. (2005). The circuitry of V1 and V2: integration of color, form, and motion.
506 *Annual Review of Neuroscience*, 28, 303-326.

507 Smith, M.A., Bair, W., & Movshon, J.A. (2002). Signals in Macaque Striate Cortical Neurons that Support
508 the Perception of Glass Patterns. *The Journal of Neuroscience*, 22 (18), 8334-8345.

509 Smith, M.A., Kohn, A., & Movshon, J.A. (2007). Glass pattern responses in macaque V2 neurons. *Journal*
510 *of Vision*, 7 (3), 5-5.

511 Tang, M.F., Dickinson, J.E., Visser, T.A.W., & Badcock, D.R. (2015). The broad orientation dependence of
512 the motion streak aftereffect reveals interactions between form and motion neurons. *Journal of Vision*,
513 15 (13), 4-4.

514 Watamaniuk, S.N., & Sekuler, R. (1992). Temporal and spatial integration in dynamic random-dot stimuli.
515 *Vision Research*, 32 (12), 2341-2347.

516 Wilson, H.R., & Wilkinson, F. (1998). Detection of global structure in Glass patterns: implications for
517 form vision. *Vision Research*, 38 (19), 2933-2947.

518 Wilson, H.R., Wilkinson, F., & Asaad, W. (1997). Concentric orientation summation in human form vision.
519 *Vision Research*, 37 (17), 2325-2330.

520 Wilson, J.A., Switkes, E., & De Valois, R.L. (2004). Glass pattern studies of local and global processing of
521 contrast variations. *Vision Research*, 44 (22), 2629-2641.

522